Original Research Article

Amelioration of paraquat-induced pulmonary fibrosis in mice by regulating miR-140-5p expression with the fibrogenic inhibitor Xuebijing

Min-na Dong[1], Yun Xiao[2], Yun-fei Li[3], Dong-mei Wang[4], Ya-ping Qu[5], Tian-wen Fang[5], Hui Li[4] and Ming-wei Liu[1] (iD)

Abstract

Intravenous Xuebijing (XBJ) therapy suppresses paraquat (PQ)-induced pulmonary fibrosis. However, the mechanism underlying this suppression remains unknown. This work aimed to analyze the miR-140-5p-induced effects of XBJ injection on PQ-induced pulmonary fibrosis in mice. The mice were arbitrarily assigned to four groups. The model group was administered with PQ only. The PQ treatment group was administered with PQ and XBJ. The control group was administered with saline only. The control treatment group was administered with XBJ only. The miR-140-5p and miR-140-5p knockout animal models were overexpressed. The gene expression levels of miR-140-5p, transglutaminase-2 (TG2), β-catenin, Wnt-1, connective tissue growth factor (CTGF), mothers against decapentaplegic homolog (Smad), and transforming growth factor-β1 (TGF-β1) in the lungs were assayed with quantitative reverse transcription polymerase chain reaction (qRT-PCR) and Western blot analysis. The levels of TGF-β1, CTGF, and matrix metalloproteinase-9 (MMP-9) in the bronchoalveolar lavage fluid were assessed by enzyme-linked immunosorbent assay (ELISA). Hydroxyproline (Hyp) levels and pulmonary fibrosis were also scored. After 14 days of PQ induction of pulmonary fibrosis, AdCMV-miR-140-5p, and XBJ upregulated miR-140-5p expression; blocked the expressions of TG2, Wnt-1, and β-catenin; and decreased p-Smad2, p-Smad3, CTGF, MMP-9, and TGF-β1 expressions. In addition, Hyp and pulmonary fibrosis scores in XBJ-treated mice decreased. Histological results confirmed that PQ-induced pulmonary fibrosis in XBJ-treated lungs was attenuated. TG2 expression and the Wnt-1/β-catenin signaling pathway were suppressed by the elevated levels of miR-140-5p expression. This inhibition was pivotal in the protective effect of XBJ against PQ-induced pulmonary fibrosis. Thus, XBJ efficiently alleviated PQ-induced pulmonary fibrosis in mice.

Keywords

matrix metalloproteinase, mice, miR-140-5p, paraquat, pulmonary fibrosis, transglutaminase-2, Xuebijing

[1]Department of Emergency, First Hospital Affiliated to Kunming Medical University, Kunming, China
[2]Intensive Care Unit, The Third Affiliated Hospital of Kunming Medical University, Kunming, China
[3]Department of Elderly Cardiovascular Diseases, First Hospital Affiliated to Kunming Medical University, Kunming, China
[4]Yunnan Green Field Biological Pharmaceutical Co., Ltd., Kunming, China

[5]Department of Postgraduate, Kunming Medical University, Kunming, China

Corresponding author:
Ming-wei Liu, Department of Emergency, The First Hospital Affiliated To Kunming Medical University, 295 Xichang Road, Wuhua District, Kunming 650032, China.
Email: lmw2004210@163.com

Introduction

Paraquat (PQ) is a nonselective contact herbicide that is extremely toxic to numerous organs when inhaled, consumed, and/or absorbed via the skin. PQ toxicity primarily affects the lungs due to the accumulation of PQ.[1–3] Such toxicity is also due to sustained redox cycling. Experiments in rats showed that oral and intraperitoneal administrations of PQ result in lung edema and hemorrhage and increase the number of alveolar macrophages with tissue damage,[4] resulting in fibroblastic proliferation. PQ-induced lung injury interrupts types I and II alveolar Clara and epithelial cells; impairs the surfactant system; and causes hemorrhage, hypoxemia, edema, and infiltration of inflammatory cells.[3,5] These pathological changes lead to respiratory failure and pulmonary fibrosis. Survivors of PQ poisoning suffer from long-term restrictive pulmonary dysfunction.[6] No effective pharmacological antidote is currently available for PQ poisoning,[5] and existing treatment methods are ineffective, resulting in high mortality.[7] Therefore, an agent with fibrosis-controlling and antioxidant qualities must be developed to treat PQ-induced lung injuries.

MicroRNAs (miRNAs) are key gene expression regulators with pivotal roles in numerous biological processes. Specific miRNA expression patterns are connected to the start and development of particular diseases, such as infections, cancers, and autoimmune and inflammatory diseases.[8–11] In addition, the gain- and loss-of-function examined by in vivo studies on miRNAs confirmed their functional importance.[10] Nevertheless, the precise roles of miRNAs in fibrotic diseases, particularly lung fibrosis, have not been thoroughly explored.[12] Previous research revealed that miR-140 is downregulated in bleomycin (BLM)-induced pulmonary fibrosis, which is negatively related to transforming growth factor-β1 (TGF-β1) activities. miR-140 overexpression could reverse TGF-β1-induced epithelial–mesenchymal transition (EMT) in A549 cells by increasing the E-cadherin level and decreasing vimentin, Smad3, and p-Smad3 expressions.[13] miR-140 is a key protective molecule against radiation-induced lung fibrosis via myofibroblast differentiation and inflammation inhibition.[14] This study aimed to determine whether miR-140 can reveal the underlying mechanisms of fibrosis for its diagnosis and therapy.

Transglutaminase 2 (TG2), a tissue transglutaminase, exhibits the largest expression pattern of all members of the transglutaminase family. TG2 has broad tissue dispersal in numerous subcellular areas and plays several roles. In rat and mouse models, TG2 promotes fibrosis in kidneys and livers.[15,16] TG2 expression is upregulated in human kidney fibrosis.[15]

A key mesenchymal feature of pathological fibrosis is the increase in fibroblast transdifferentiation, particularly transdifferentiation into myofibroblasts. The myofibroblasts with the qualities of smooth muscle cells and fibroblasts can improve the synthesis of an atypical matrix in pulmonary fibrosis; they also overexpress α-smooth muscle actin (α-SMA).[17] TGF-β1 plays a primary role in pulmonary fibrosis. It engages and enhances fibroblast proliferation and prompts the EMT of alveolar epithelial cells by stimulating the mothers against decapentaplegic homolog (Smad)-signaling pathway.[18]

Xuebijing (XBJ), a traditional Chinese medicinal herb, has been successfully utilized in the treatment of inflammation-related diseases.[19–21] The medicinal preparation of XBJ has been identified, but the underlying mechanisms remain unclear.[19] The specific effects of XBJ on several immunomodulatory processes and factors have been reported.[20] PQ poisoning is due to systemic inflammation and excessive fibrosis-related immune response. XBJ treatment significantly improved pulmonary fibrosis[22] and focal segmental glomerular fibrosis in BLM-induced rats.[23] XBJ treatment also decreased TGF-β and type III procollagen peptide (PIIIP) levels and increased the 28-day survival rate of patients with moderate PQ poisoning.[24] Intravenous XBJ therapy can be used for fibrillation-connected diseases and as an experimental tool to determine immune factors that cause serious sickness and death in PQ-induced fibrosis.

The improved activation of the canonical Wnt signaling pathway could play a pivotal role in fibrogenesis.[25] The pathological activation of canonical Wnt signaling is connected to the pathogenesis of dermal, renal, liver, and pulmonary fibrosis.[26] Scholars have reported the enhanced staining of β-catenin in the nuclei of bronchiolar lung epithelial and type II alveolar epithelial cells from humans with idiopathic pulmonary fibrosis (IPF) lung biopsies.[27] Microarray analysis indicated that the elevated expression of genes was linked to the Wnt/β-catenin pathway in IPF,[28–30] which was consistent with the findings in this

study. β-catenin is moved into the nucleus, where it binds to the T-cell factor/lymphoid enhancer-binding factor (Tcf/Lef) and prompts the transcription of Wnt target genes.[31]

Although several factors and pathways promote or limit the development of lung fibrosis, effective therapeutic methods for the treatment of lung fibrosis are unavailable. In this study, intravenous XBJ therapy was used for PQ poisoning in mice, and its efficacy was assessed. The effects of intravenous XBJ therapy on TG2, Wnt/β-catenin signaling, TGF-β1, Smad2, Smad3, and α-SMA via miR-140-5p expression modulation were analyzed to determine the pathways and immune factors pivotal to PQ pathogenesis and XBJ targets. The ability of miR-140 to regulate the development and progression of pulmonary fibrosis by regulating the Wnt/β-catenin pathway was explored.

Materials and methods

Mice

Eighty C57BL/6J mice were obtained from the Kunming Medical University Laboratory Animal Center (Kunming, China) and kept in a pathogen-free area in the Animal Care Facility of Kunming Medical University. The mice were 8–9 weeks old and weighed 20–30 g. They were kept in a vivarium at 23°C with a 12 h light/12 h dark cycle (lights are off at 7:00 p.m.). The mice were also given a standard laboratory diet and water, and they ate and drank ad libitum. The study was endorsed by the Ethics Committee of Kunming Medical University (approval No. KYYM-2018-012-E23) and performed in accordance with the Guidelines of the Animal Care Committee of Kunming Medical University. All applicable international, national, and/or institutional guidelines for the care and use of animals were followed.

Cell culture

The A549 human lung epithelial cell line (Heilongjiang Cancer Institute, Harbin, China) was propagated in Dulbecco's modified eagle medium (DMEM) supplemented with 5% fetal bovine serum, 100 U/mL of penicillin, 100 U/mL of streptomycin, and 50 μg/L of amphotericin B. Cultures were incubated in a humidified environment with 5% CO_2 at 37°C. Cells were sub-cultured in six-well plates and incubated until they were subconfluent.

Mimics and inhibitors of gene transfection and miRNA

Cells were cultured in six-well plates until 40% confluency was achieved. For transfection, miR-140-5p mimic, miR-140-5p mimic-negative control (NC), miR-140-5p inhibitor, and miR-140-5p inhibitor-NC were mixed individually with Lipofectamine 2000 (Invitrogen, Carlsbad, CA, USA). The solutions were placed in the cell culture medium in accordance with the manufacturer's directions. After 48 h of transfection, proteins and total RNA were separated from the cells and quantified via Western blot and quantitative reverse transcription polymerase chain reaction (qRT-PCR) analyses.

Determination of cell transfection efficiency

As previously described,[32] cells were grown on glass coverslips and fixed with 4% sucrose and 4% paraformaldehyde after transfection for 48 h. They were then permeabilized for 10 min with 0.1% Triton X-100. The cells were rinsed and mounted on cover glasses with 4,6-diamidino-2-phenylindole (Invitrogen, Carlsbad, CA, USA) and Prolong Gold anti-fade reagent. The cells were visualized under an Olympus IX 81 microscope (Olympus, Tokyo, Japan). The percentage of green fluorescent cells among all cells was observed, and transfection efficiency was calculated using the following equation: transfection efficiency = number of green fluorescent cells visible in the visual field/total number of cells × 100.

In vivo miR-140-5p knockdown and miR-140-5p expression mouse model

A construct that expressed constitutively active miR-140-5p with 1×109 plaque-forming units (PFU) of AdCMV-miR-140-5p was intravenously injected into the tail once a day for 14 days to establish a miR-140-5p expression mouse (n = 8). Intraperitoneal PQ challenge (10 mg/kg) was conducted after 14 days to establish a miR-140-5p expression model mouse (n = 8). Anti-miR-140-5p oligonucleotides and locked nucleic acid-modified scrambled oligonucleotides (Exiqon, Woburn, MA, USA) were diluted in saline solution (5 mg/mL). The solution at 10 mg/kg was administered to the mice via intraperitoneal injection to establish a miR-140-5p knockdown mouse (n = 8). After a minimum

of 30 min, the mice were exposed to PQ (10 mg/kg) for 14 days[12] to establish a miR-140-5p knockdown model mouse (n=8). The saline was injected into the control mice (n=8). The model mouse (n=8) were treated with PQ (10 mg/kg) by intraperitoneal injection for 14 days to induce pulmonary fibrosis model. After 14 days of PQ injection, the mice were anesthetized with intravenous pentobarbital sodium (30 mg/kg) and sacrificed via cervical dislocation. Their lungs were obtained, used for real-time PCR and Western blot analyses, stained with Masson's trichrome and hematoxylin and eosin (H&E) to observe pathological changes in lung tissue.

miR-140-5p target gene prediction and dual-luciferase reporter assay

Two software applications, one database (www.mirbase.org), PicTar (www.pictar.org), and Target Scan (http://www.targetscan.org) were used to determine the possible miR-140-5p targets. A549 human lung epithelial cells (1×105) were cultured in 24-well plates and transfected using Lipofectamine 2000 (Invitrogen, Carlsbad, CA, USA) with one of the following: Wnt 1-3′UTR-wt, Wnt-3′UTR-mt, miR-140-5p, or mi-NC. At 24 h post-transfection, luciferase activity was determined using the Dual-Luciferase Reporter Assay System (Promega, Madison, WI, USA). The results were normalized to *Renilla* luciferase activity.

Drugs

XBJ, which consists of Honghua (Flos Carthami), Chishao (Radix Paeoniae Rubra), Danshen (Radix Salviae Miltiorrhizae), and Chuanxiong (Rhizoma Chuanxiong), was obtained from Tianjin Chase Sun Pharmaceutical Co., Ltd. (No. Z20040033). XBJ was set up for injection as described previously.[17,19] Each 10 mL of XBJ injection had 1 g of the crude drug, which was identified by determining its active compounds and biochemical fingerprints.[17,19] According to our previous study,[17] the active ingredients in XBJ are ligustrazine, ferulic acid, safflor yellow A, tanshinol, and paeoniflorin.

Experimental design and PQ-induced pulmonary fibrosis

Thirty-two mice were weighed and arbitrarily grouped into four to determine the protective effects of XBJ against pulmonary fibrosis. Each group consisted of eight mice. PQ (10 mg/kg) was administered by intraperitoneal injection to induce pulmonary fibrosis in mice.[33] Saline was administered as control. Group 1 (n=8), the control group, was untreated or was treated with saline only. Group 2 (n=8), the treatment control group, was treated with 8 mL/kg of XBJ via tail vein injection once each day. Group 3 (n=8), the model group, was administered with PQ (10 mg/kg) to prompt pulmonary fibrosis. According to the previously described approach,[18,21] Group 4 (n=8), the treatment group, was treated with PQ and 8 mL/kg of XBJ via tail vein injection once each day to prompt pulmonary fibrosis.[18] After 14 days of PQ injection, the mice were anesthetized with intravenous pentobarbital sodium (30 mg/kg) and sacrificed via cervical dislocation. Their lungs were obtained, and a tiny portion of each lung was first fixed in 10% formalin and embedded in paraffin for Masson's trichrome staining and H&E staining.

Collection of bronchoalveolar lavage tissue, fluid, and samples

Midline thoracotomy was performed. Blood (3 mL) was collected from the heart and centrifuged at 4°C and $2000 \times g$ for 10 min. The resulting serum was frozen at −80°C until use. The mice were first anesthetized and the lungs were lavaged four times with 1 mL of sterile saline to obtain the bronchoalveolar lavage (BAL) fluid. The total lavage liquid was pooled and used for every mouse. Lavage specimens were promptly centrifuged at room temperature for 10 min at $2000 \times g$ and stored at −80°C for subsequent use. The right middle lung lobes were stored in liquid nitrogen (−80°C). The right lower lobes were histologically examined.

Real-time PCR

Lung tissues were frozen in liquid nitrogen and kept at −80°C until the total RNA was removed with a TRIzol reagent. RNA was amplified using a single-step PCR kit (Promega, Madison, WI, USA) in accordance with the manufacturer's directions. Real-time qRT-PCR was conducted in a 20-μL reaction system with 50 mM KCl, 20 mM Tris-HCl, 1.25 mM $MgCl_2$, 0.2 mM dNTP, 0.5 mM primer, 0.5 μL of cDNA, and 1 U Taq DNA polymerase in an ABI7700 sequence detector (Applied Biosystems, Foster City, CA, USA). PCR primers (Table 1) for TG2, human epididymis protein 4

Table 1. Primer sequences for analysis by qRT-PCR.

Genes	Primers
miR-140-5p	F-5′-GAGTGTCA-GTGGTTTTACCCT-3′ R-5′-GCAGGGTC-CGAGGTATTC-3′
U6	F-5′-GTGCTCGCTTCGGCAGCACATATAC-3′ R-5′-AAAAATATGGAACGCTCACGAATTTG-3′
TG-2	F-5′-CAAGAACAAGGCAGACTTATCGC-3′ R-5′-TCTGATTATCTCGCACCAGGAAG-3′
β-catenin	F-5′-CCAGAGTGAAAAGAACGGTAGC-3′ R-5′-GAACCGCTCATTGCCGATAG-3′
Wnt-1	F-5′-ACATCAAGGCAGGGAAGAAAT-3′ R-5′-TCTGGACACTGGAAATCA-3′
TGF-β1	F-5′-CTGCTGACCCCCACTGATAC-3′ R-5′-CTGTATTCCGTCTCCTTGGTTC-3′
Smad2	F-5′-ATCTTGCCATTCATCCCGCC-3′ R-5′-CTGTTCTCCACCACCTCGTC-3′
Smad3	F-5′-TGGGCAAGTTCTCCAGAAGTT-3′ R-5′-AGGATGACGACATGCTG-3′
HE4	F-5′-CCGACAACCTCAAGTGCTG-3′ R-5′-CGAGCTGGGGAAAGTTAATG-3′
β-actin	F-5′-GACAGGATGCAGAAGGAGATTACT-3′ R-5′-TGATCCACATCTGCTGGAAGGT-3′

(HE4), Wnt-1, α-SMA, β-catenin, TGF-β1, Smad2, and Smad3 were utilized in this evaluation. The PCR cycle parameters were as follows: 95°C for 3 min, followed by 25 cycles of 98°C for 30 s, 60°C for 40 s, and 72°C for 60 s, followed by a final extension at 72°C for 5 min. The PCR products were isolated on 2% Agarose gels. β-actin was used as an endogenous control. The values in each specimen were normalized against the β-actin content. mRNA expression levels of the target genes were determined through the $2^{-\Delta\Delta Ct}$ method.[34,35] miR-140-5p was identified with qRT-PCR.[7] A looped antisense primer (Table 1) was utilized for reverse transcription. The reverse transcription reaction was diluted 10 times and used as the template for qRT-PCR. The reactions were performed in 96-well optical plates, and the cycle was as follows: 95°C for 1 min, followed by 35 cycles of 95°C for 15 s, 56°C for 15 s, and 72°C for 25 s. The cycle threshold (Ct) was documented and the quantity of miR-140-5p with regard to U6 RNA was determined in accordance with the mathematical expression of $2^{-(CtmiRNA2CtU6RNA)}$.

Western blot analysis

The lungs were homogenized in lysis buffer with 150 mM NaCl, 0.5% sodium deoxycholate, 50 mM Tris-HCl, 0.1% sodium dodecylsulphate (SDS), 1% NP-40, 2 mM NaF, 2 mM ethylenediaminetetraacetic acid (EDTA), and a protease inhibitor cocktail tablet (Roche Applied Science, Indianapolis, IN, USA). Protein concentrations were determined via the bicinchoninic acid assay (Pierce Biotechnology, Inc., Rockford, IL, USA). Protein samples (30 mg) from each group were placed into the lanes of 12% Tris-glycine polyacrylamide gels and prestained molecular weight markers (Bio-Rad, Hercules, CA, USA). Then, the protein samples were electrophoresed and electrophoretically moved onto polyvinylidene difluoride membranes (Millipore Corp., Marlborough, MA, USA). The subsequent membranes were halted with 5% bovine serum albumin at room temperature for 1 h and incubated overnight at 4°C with primary antibodies to reach a dilution ratio of 1:1000 in Tris-buffered saline with Tween-20 (TBST; Pierce, Rockford, IL, USA). Such antibodies include anti-collagen-III, anti-Smad3, anti-matrix metalloproteinase-9 (MMP-9), anti-Smad2, anti-p-Smad3, anti-p-Smad2, anti-connective tissue growth factor (CTGF), anti-TG2, and anti-platelet-derived growth factor (PDGF) from cell signaling (Beverly, MA, USA), as well as anti-β-actin and anti-collagen-I from Santa Cruz. β-actin was used as a constitutive control to verify the fact that identical portions of proteins were added. The membranes were incubated with appropriate horseradish peroxidase-linked anti-rabbit antibodies after rinsing with TBST (Pierce, Rockford, IL, USA) to a dilution ratio of 1:20,000 in TBST for 1 h at room temperature. Immunoreactive bands were examined with enhanced chemiluminescence and quantified by densitometry with the Bio-Rad Universal Hood and Quantity One software (Bio-Rad) after rinsing with TBST. All outcomes were normalized to β-actin levels lane by lane.

Immunohistochemistry

The lungs were inflated to a constant pressure of 25 cm H_2O. Then, 4% paraformaldehyde was installed in the trachea. Subsequently, the lungs were immersed in 70% ethanol for 24 h and paraffin-embedded.[34] Following antigen retrieval with Retrievagen A (Zymed, South San Francisco, CA, USA), the lung sections were immunostained for 20 min at 100°C, and 3% hydrogen peroxide was used to quench endogenous peroxidases. Staining was arrested by phosphate-buffered saline (PBS) containing 2% bovine serum albumin. The sections were then stained with anti-α-SMA and HE4 antibodies, along with primary anti-TG2 (BD

Pharmingen, San Jose, CA, USA) for 1 h at room temperature. The sections were rinsed and incubated with secondary antibodies (R&D Systems, Minneapolis, MN, USA). Vectastain ABC (Vector Labs, Burlingame, CA, USA) and 3,3′-diaminobenzidine (Vector Labs) were used for the development. Five fields at high power (200×) were chosen on each slide following staining, and the average size of the area of positive expression in every field was determined using a true color multi-functional cell image analysis management system (Image-Pro Plus; Media Cybernetics, Rockville, MD, USA). Values were expressed as positive units.

In situ hybridization (ISH)

miR-140-5p expression in lung tissues was evaluated by designing a 5′-digoxigenin-labeled oligonucleotide probe to hybridize with miR-140-5p in situ using the microRNA ISH buffer and control kits (Wuhan Boster Biological Technology, Wuhan, China). The kit instructions were strictly followed.

Quantification of TGF-β1, HE4, and CTGF in BAL and HE4, laminins, and hyaluronan in plasma by ELISA

The primary antibodies against TGF-β1, HE4, hyaluronan (HA), laminins (LN), and CTGF (R&D Systems, Minneapolis, MN, USA) were applied to Nalgene Nunc MaxiSorp plates at room temperature for 1 h and rinsed with 0.5% Tween-20 and PBS. The specimens were placed onto the plates (which were previously blocked with casein) and incubated at room temperature for 1 h. The specimens were rinsed with distilled H_2O containing 0.01% Tween-20, and the wells were loaded with biotinylated secondary antibodies and allowed to react for 1 h. This process was followed by treatment with streptavidin–horseradish peroxidase conjugate (Jackson ImmunoResearch, West Grove, PA, USA) diluted to 1:20,000. The reaction was conducted with 0.01% tetramethylbenzidine dissolved in 0.5% hydrogen peroxide and dimethyl sulfoxide and analyzed by endpoint spectrometry.

Total collagen levels in the lungs

The total collagen content in the lungs was determined in accordance with the total soluble collagen levels (Sircol Collagen Assay, Biocolor, Ireland). The left lung was homogenized in 5 mL of 0.5 M acetic acid with pepsin (1 mg/10 mg tissue; Sigma-Aldrich,

St. Louis, MO, USA) and incubated at 24°C for 24 h under stirring for 240 r/min. Sircol dye was included (1 mL/100 mL). The samples were incubated for 30 min. The samples were centrifuged for 12 min at 12,000 r/min. A total of 1 mL of 0.5 M NaOH was used to resuspend the subsequent pellets. The optical densities were quantified with a spectrophotometer at 540 nm.

Hydroxyproline assay

As described previously,[36] hydroxyproline (Hyp) content was determined in the lung tissue samples (40 mg per mouse lung, wet weight) to assess collagen accumulation. The Hyp assay was conducted with a Hyp test kit purchased from Nanjing Jiancheng Bioengineering Institute (Nanjing, China). The test was performed in accordance with the manufacturer's instructions.

Histopathology

The middle lung lobes were processed as follows: the samples were embedded in paraffin, fixed with 10% buffering formalin, were cut into 4-mm-thick sections, and stained with Masson's trichrome. Lung fibrosis severity among the groups was evaluated using the Ashcroft score.[37] Thirty regions with a magnification of 100× were arbitrarily selected in every specimen. The mean score for the fields was utilized as the fibrosis score for that sample. Samples were scored blindly.

Statistical analyses

Statistical analyses were carried out with SPSS (version 15.0, Chicago, IL, USA). Data are shown as the mean ± standard deviation (SD) of three samples from three independent experiments, as specified in the figure legends. Statistically significant differences between the treatment and control groups or model group were determined using Student's t-test. Data sets with several comparisons were examined using one-way ANOVA with Dunnett's post-tests. P-values < 0.05 were considered statistically significant.

Results

Transfection efficiency and mimics or inhibitor stability

The percentage of green fluorescent cells in all cells was observed, and transfection efficiency

was calculated to observe the transfection efficiency and stability of the mimics, control, or inhibitor. As shown in Figure 1, the transfection efficiencies of miR-140-5p mimics, miR-140-5p mimic-NC, miR-140-5p inhibitor, and miR-140-5p inhibitor-NC were over 90%. The levels of miR-140-5p in the mimics, control, or inhibitor were measured by RT-PCR. The miR-140-5p levels in the mimics were significantly higher than those of the control mimic. The miR-140-5p levels in the inhibitor were significantly lower than those of the control inhibitor. Thus, the transfection efficiencies and the stability of the mimics or inhibitor were high.

Smad/TGF-β1 and Wnt1/β-catenin signaling pathways are significantly downregulated by miR-140-5p in A549 cells

The Smad/TGF-β1 and Wnt1/β-catenin signaling pathways are the two key pathways in pulmonary fibrosis.[9] miR-140-5p mimics, miR-140-5p mimic-NC, miR-140-5p inhibitor, and miR-140-5p inhibitor-NC were mixed individually with Lipofectamine 2000 (Invitrogen, Carlsbad, CA, USA) and placed in the cell culture. The expression levels at 24 h post-transfection Wnt1, β-catenin, p-Smad3, and TGF-β1 were quantified via Western blot analysis. The elevated miR-140-5p levels in A549 cells significantly decreased Wnt1, β-catenin, p-Smad3, and TGF-β1 expressions ($P < 0.05$). Thus, miR-140-5p could modulate the Smad/TGF-β1 fibrogenic signaling pathway.

Overexpression of miR-140-5p inhibited PQ-induced pulmonary fibrosis

An active miR-140-5p expression construct was created to examine the effects of miR-140-5p overexpression on PQ-induced pulmonary fibrosis. The construct was administered to the mice via the tail vein through 1×109 PFU injection of AdCMV-miR-140-5p. After 14 days, an intraperitoneal PQ (10 mg/kg) challenge was conducted for 14 days. A marked reduction in inflammatory cell infiltration and collagen deposition was noted in the lungs of PQ-treated miR-140-5p mice in contrast to those of control mice following histopathological examination (Figure 2). The elevation in AdCMV-miR-140-5p expression may attenuate PQ-induced pulmonary fibrosis.

PQ-induced pulmonary fibrosis worsened in miR-140-5p knockdown mice

A PQ-induced pulmonary fibrosis mouse model was used to explore the role of miR-140-5p in fibrosis caused by noninfectious lung injury. WT B6 and miR-140-5p knockdown mice were exposed to PQ by intratracheal instillation and sacrificed after 14 days. Male 8 week-old miR-140-5p knockdown and B6 control mice were treated with 10 mg/kg of PQ. Twenty-one days after exposure to PQ, fibrosis was assessed. Histopathological evaluation of the lungs of PQ-treated miR-140-5p knockdown mice demonstrated enhanced inflammatory cell infiltration and collagen deposition in contrast to the WT mice (Figure 2). Sircol assays indicated a significant reduction in total lung collagen in PQ-treated miR-140-5p knockdown mice in contrast to that of the WT controls. Thus, the reduction in miR-140-5p expression may be involved in attenuating PQ-induced pulmonary fibrosis.

Impacts of miR-140-5p on Wnt1, β-catenin, collagen-I, TGF-β1, and TG2 in lung tissues with PQ-induced pulmonary fibrosis

A PQ-induced pulmonary fibrosis mouse model was used to examine the role of miR-140-5p in PQ-induced fibrosis. PQ was administered via intratracheal instillation to miR-140-5p overexpressing, WT B6, and miR-140-5p knockdown mice, and the animals were sacrificed after 21 days. As shown in Figure 3, the mice that received 1×109 PFU of AdCMV-miR-140-5p had significantly higher miR-140-5p expression levels than the control. The treatment blocked TG2 and β-catenin expressions. By contrast, miR-140-5p knockout markedly reduced miR-140-5p expression levels and remarkably increased TG2 and β-catenin expression in the lungs of mice exposed to PQ.

Wnt1 are direct targets of miR-140-5p

A well-known database that can predict the likely targets of miR-140-5p was used to determine how miR-140-5p mediated PQ-induced pulmonary fibrosis. Wnt1 is an important fibrotic regulator of PQ-induced pulmonary fibrosis. The Wnt1 mRNA and protein levels were dramatically reduced after
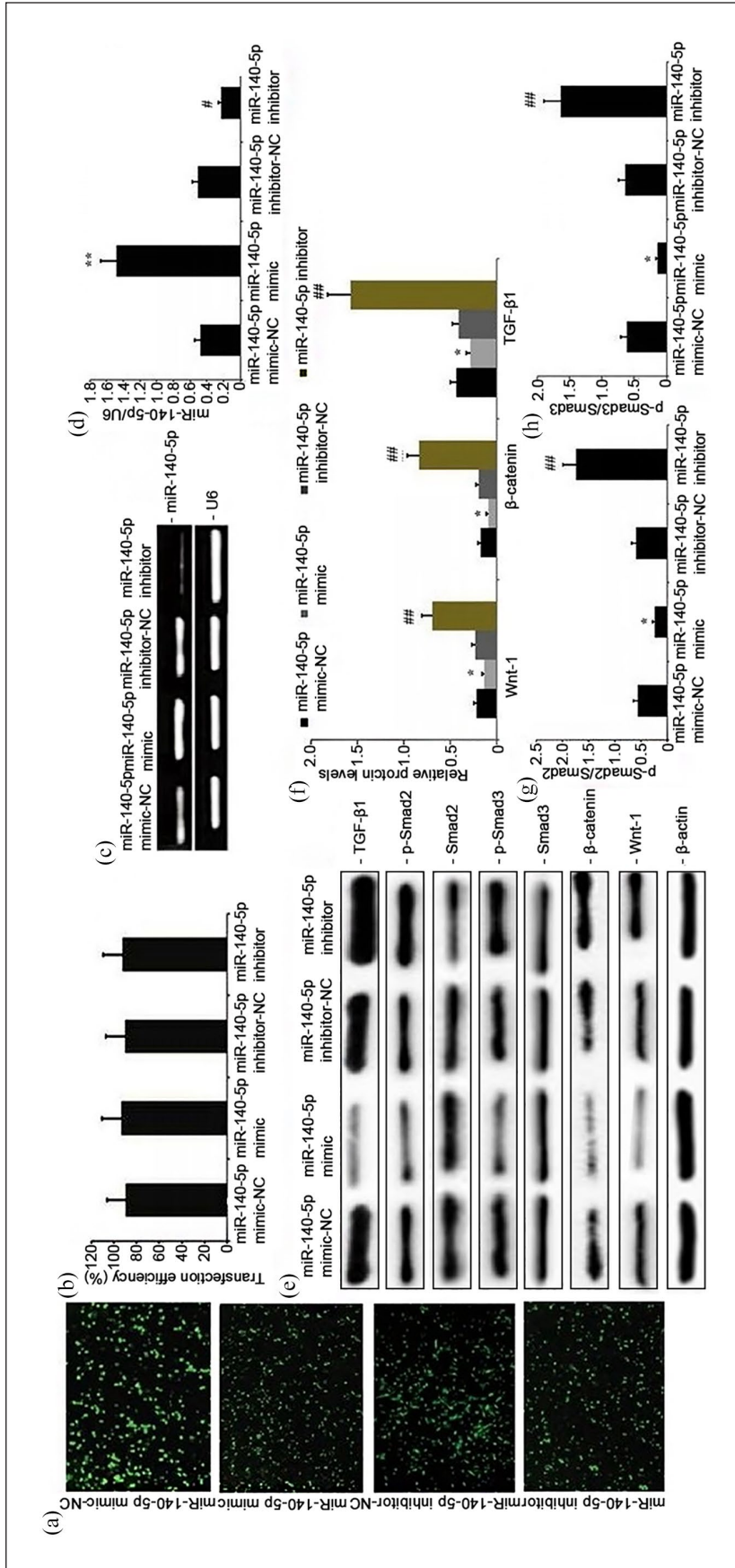
Figure 1. Transfection efficiency and stability of the mimics or inhibitor and effects of miR-140-5p in A549 cells on the Smad/TGF-β1 and Wnt1/β-catenin signaling pathways. miR-140-5p mimics, miR-140-5p mimic-NC, miR-140-5p inhibitor, and miR-140-5p inhibitor-NC were individually mixed with Lipofectamine 2000 (Invitrogen, Carlsbad, CA, USA) and placed into the cell culture to transfect A549 cells. After 48 h of transfection, (a) fluorescence expression of transfected cells after miR-140-5p mimics, miR-140-5p mimic-NC, miR-140-5p inhibitor, and miR-140-5p inhibitor-NC transfection (×50); (b) transfection efficiency of miR-140-5p mimics, miR-140-5p mimic-NC, miR-140-5p inhibitor, and miR-140-5p inhibitor-NC; (c) and (d) relative miR-140-5p expression levels were determined by qRT-PCR; (e)–(h) Wnt1, β-catenin, p-Smad2, p-Smad3, and TGF-β1 expression levels were measured by Western blot analysis. Data from three independent experiments are presented as mean ± SD.

*$P < 0.05$ versus control mimic.
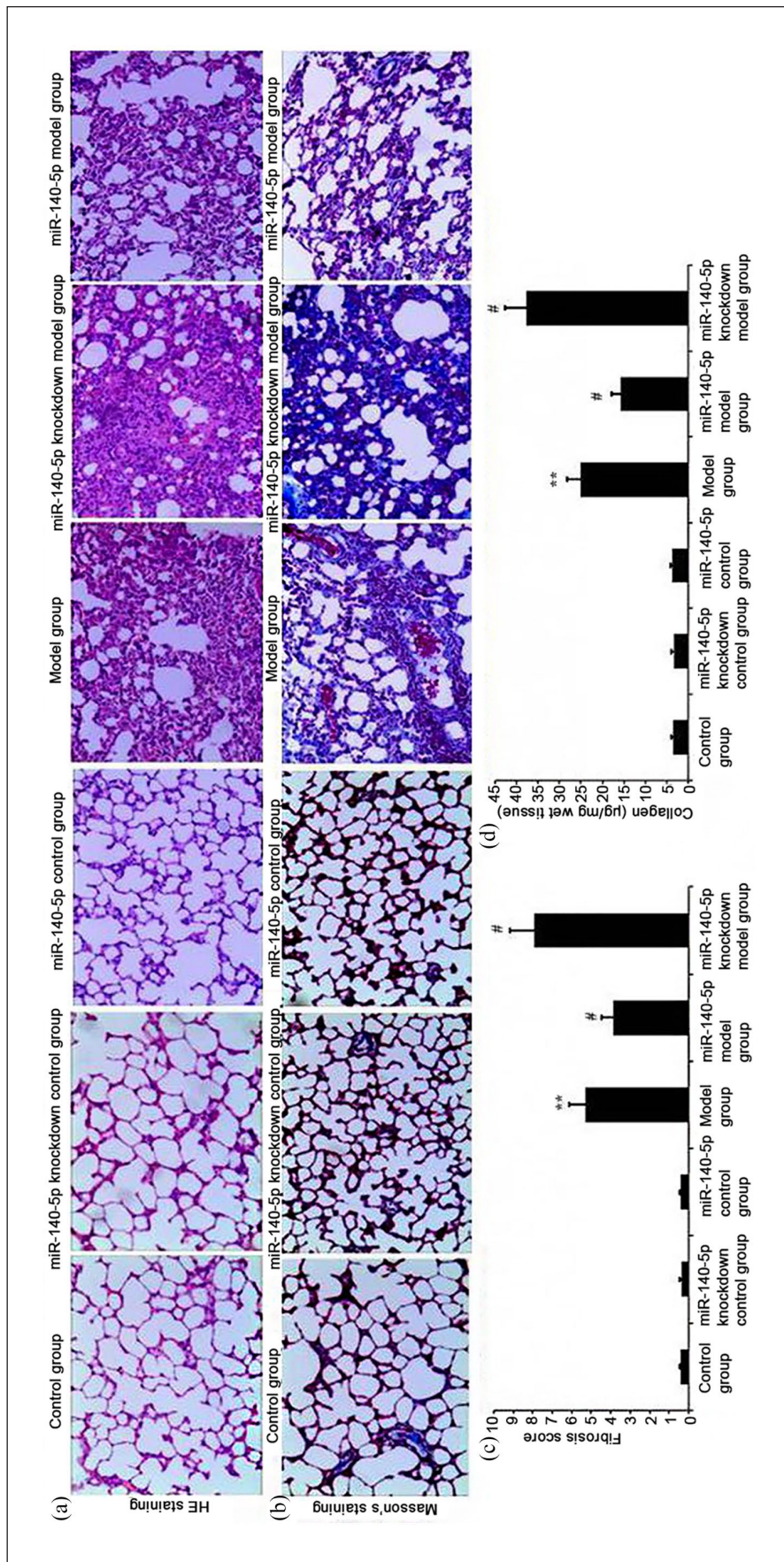#$P < 0.05$ versus control inhibitor.

Figure 2. Effects of miR-140-5p overexpression on PQ-induced pulmonary fibrosis. Active miR-140-5p expression construct was administered to the mice via tail veins through the injection of 1×10^9 PFU of AdCMV-miR-140-5p along with the intraperitoneal delivery of PQ. After 14 days, the intraperitoneal PQ (10 mg/kg) challenge was performed for 14 days. The role of miR-140-5p knockdown in fibrosis caused by noninfectious lung injury was explored using WT B6 and miR-140-5p knockdown mice exposed to PQ by intratracheal instillation and sacrificed after 14 days. Histopathological examination of the lungs was performed. (a) and (b) Representative images of Masson's trichrome-stained lung sections from the three experimental groups (magnification, 400×). (c) and (d) Pulmonary fibrosis scores and collagen levels expressed as mean ± SD from three experiments with three replicates.

**$P < 0.01$ versus the control group, the control miR-140-5p group, and the control miR-140-5p group.

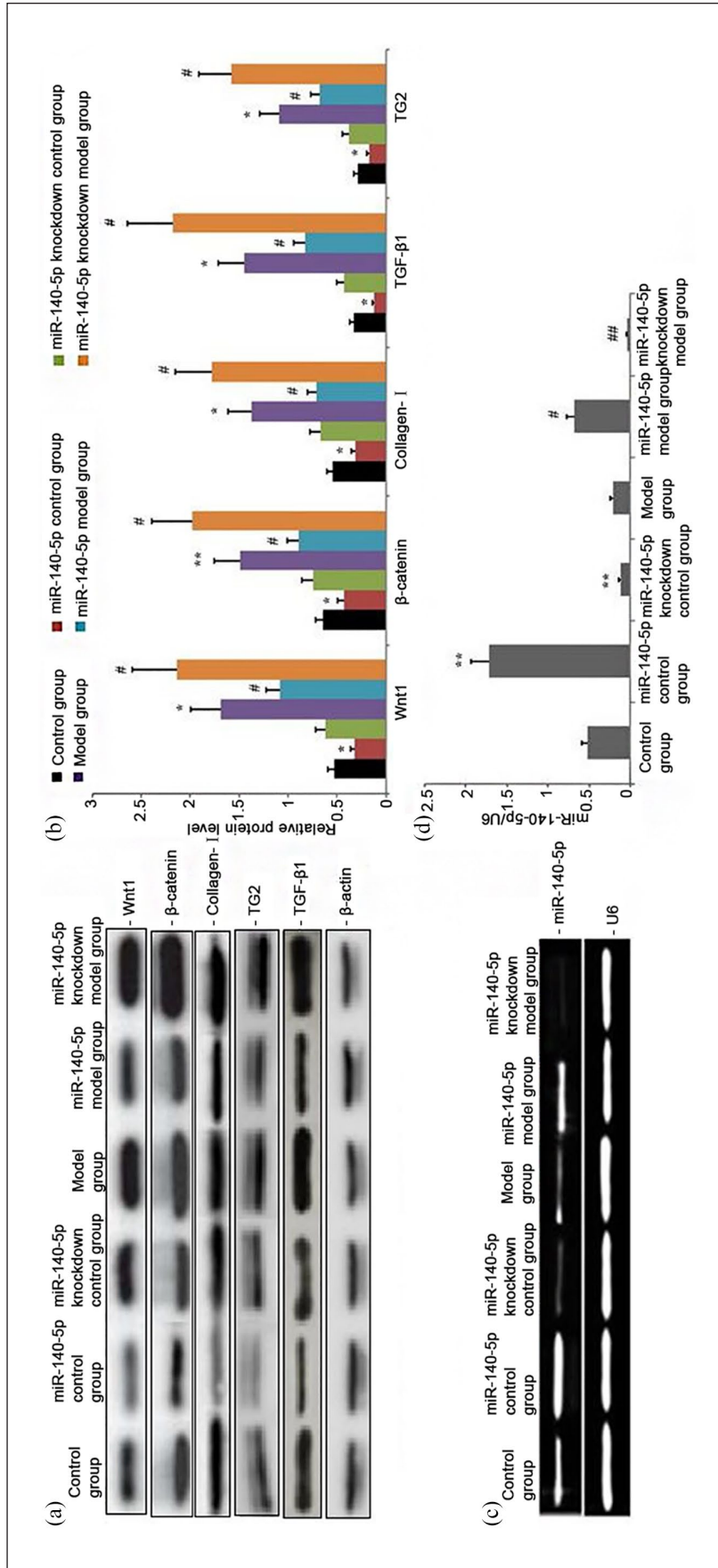\#$P < 0.05$ versus the model group.

Figure 3. Effects of miR-140-5p on Wnt1, β-catenin, collagen-I, TGF-β1, and TG2 expression in pulmonary fibrotic tissue induced by PQ. WT B6, miR-140-5p overexpression, and miR-140-5p knockdown mice were exposed to PQ by intratracheal instillation and sacrificed after 21 days. The expression of miR-140-5p was measured by qRT-PCR. TG2 and β-catenin levels in the lungs were measured by Western blot analysis. Quantitative densitometry data from three independent experiments are presented as mean ± SD.
$*P < 0.05$, $**P < 0.01$ versus the control group.
$\#P < 0.05$, $\#\#P < 0.01$ versus the model group.
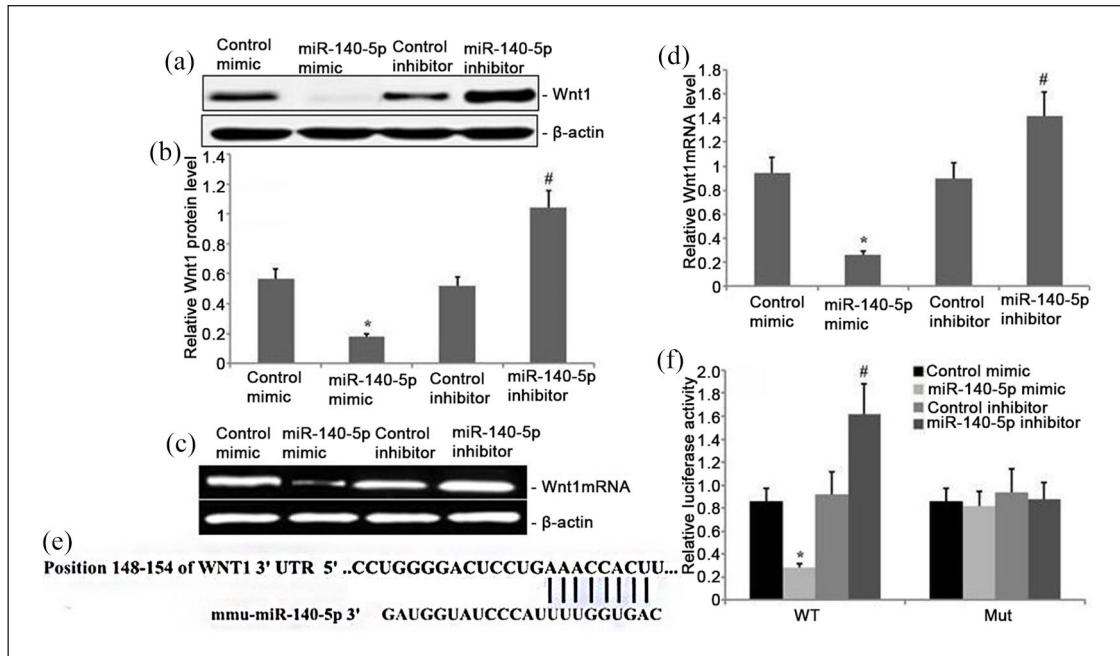$P > 0.05$ the control mice versus the control treatment group.

Figure 4. Wnt1 is a downstream target of miR-140-5p. (a) Reduced mRNA levels of Wnt1 in the A549 human lung epithelial cells after miR-140-5p overexpression ($P < 0.05$); levels were enhanced after miR-140-5p downregulation ($P < 0.05$). (b) Wnt1 was decreased in cells with miR-140-5p overexpression when compared with the empty vector control ($P < 0.05$). Wnt1 was significantly increased in cells with miR-140-5p downregulation. (c) miR-140-5p bound to the 3'-UTR regions of Wnt1 and binding was interrupted in mutant Wnt1. (d) Dual-luciferase reporter assay indicated that miR-140-5p mimic bound to the 3'-UTR region of the wild-type Wnt1, rather than the Wnt1 mutants ($P < 0.05$).

miR-140-5p overexpression (Figure 4(a)–(d)). The interaction between miR-140-5p and Wnt1 was validated by constructing wild-type and mutant Wnt1 for a dual-luciferase reporter assay (Figure 4(e)–(f)). As hypothesized, miR-140-5p became bound to the wild-type Wnt1 rather than to the mutants (Figure 4(f)).

XBJ administration upregulated miR-140-5p expression in mice with PQ-induced pulmonary fibrosis

The effects of XBJ administration on miR-140-5p expression in fibrotic lung tissues from mice treated with XBJ and PQ for 14 days were explored. miR-140-5p expression in pulmonary tissues was measured by qRT-PCR and ISH. miR-140-5p expression was decreased in the lungs in PQ-induced pulmonary fibrosis (Figure 5). Conversely, miR-140-5p expression was significantly increased in XBJ-treated mice. ISH showed the miR-140-5p expression in the cytoplasm of macrophages, lung alveolar epithelial type II cells, hyperplastic bronchiolar epithelial cells, and fibroblasts. However, no difference

was found between the control and the control treatment groups.

XBJ administration halted the gene and protein expression of TG2, HE4, Wnt-1, β-catenin, Smad3, Smad2, and TGF-β1 in mice with PQ-induced pulmonary fibrosis

The effects of XBJ on TG2, HE4, Wnt-1, β-catenin, Smad3, Smad2, and TGF-β1 were determined by examining their gene expression and protein levels in mouse pulmonary tissues using qRT-PCR and Western blot analysis, respectively. The model group had greater TG2, HE4, Wnt-1, β-catenin, Smad3, Smad2, and TGF-β1 gene expressions, as well as TG2, HE4, Wnt-1, β-catenin, p-Smad3, p-Smad2, and TGF-β1 protein levels ($P < 0.05$; Figure 6) compared with the control group. Nevertheless, XBJ delivery halted the elevation in TG2, HE4, Wnt-1, β-catenin, Smad3, Smad2, and TGF-β1 gene and TG2, HE4, Wnt-1, β-catenin, p-Smad3, p-Smad2, and TGF-β1 protein expressions. However, no difference was found between the control and the control treatment groups.
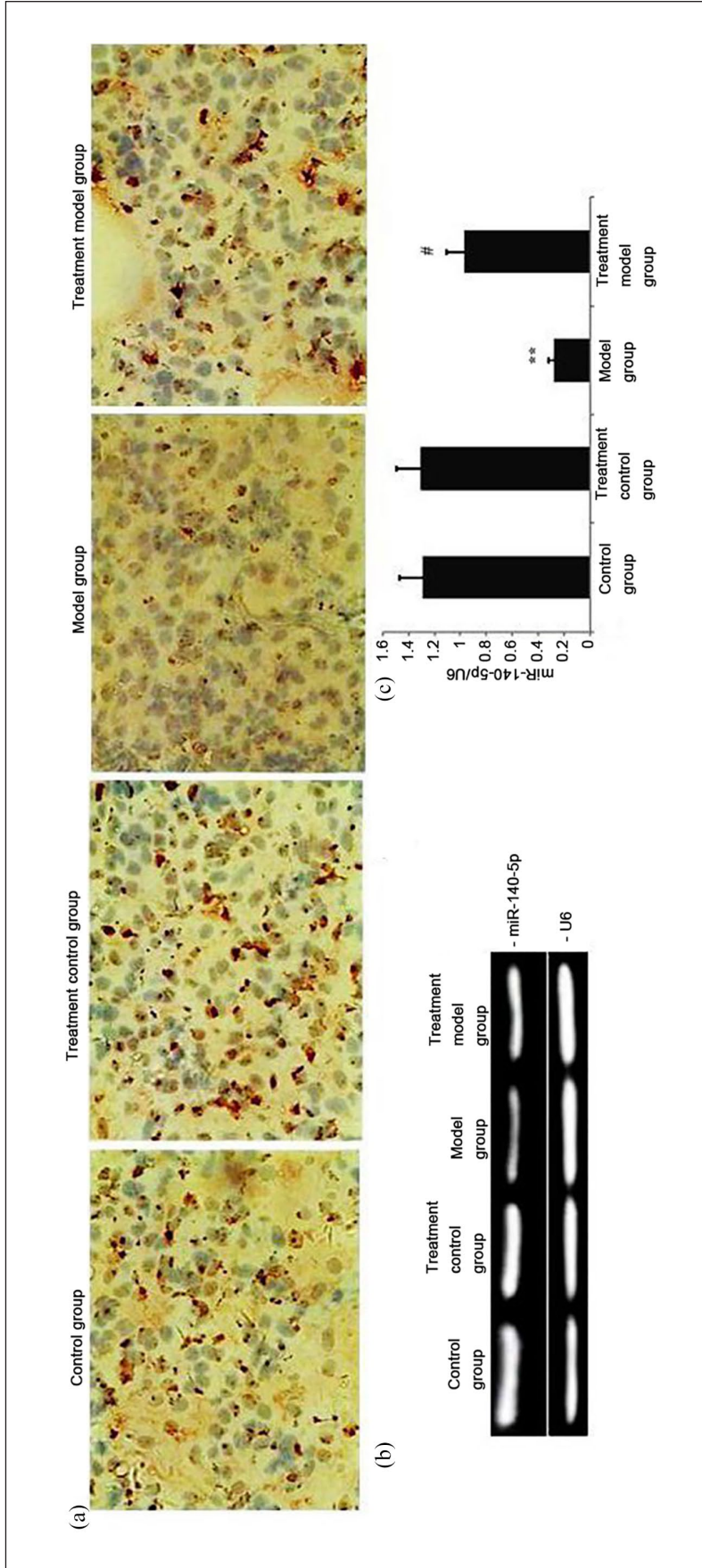
Figure 5. Effects of XBJ administration on miR-140-5p expression during PQ-induced pulmonary fibrosis. Mice were treated with XBJ and PQ for 14 days, and miR-140-5p expression was determined by ISH. (a) ISH images from the four treatment groups are indicated with arrows (magnification: 400×): the macrophages, lung alveolar epithelial type cells, hyperplastic bronchiolar epithelial cells, and fibroblasts on the image were identified under a light microscope GVC (220 V, 50 Hz). (b) and (c) Relative miR-140-5p expression levels were determined by qRT-PCR; bars indicate mean ± SD.

*$P < 0.05$, **$P < 0.01$ versus controls

#$P < 0.05$ versus the model group.
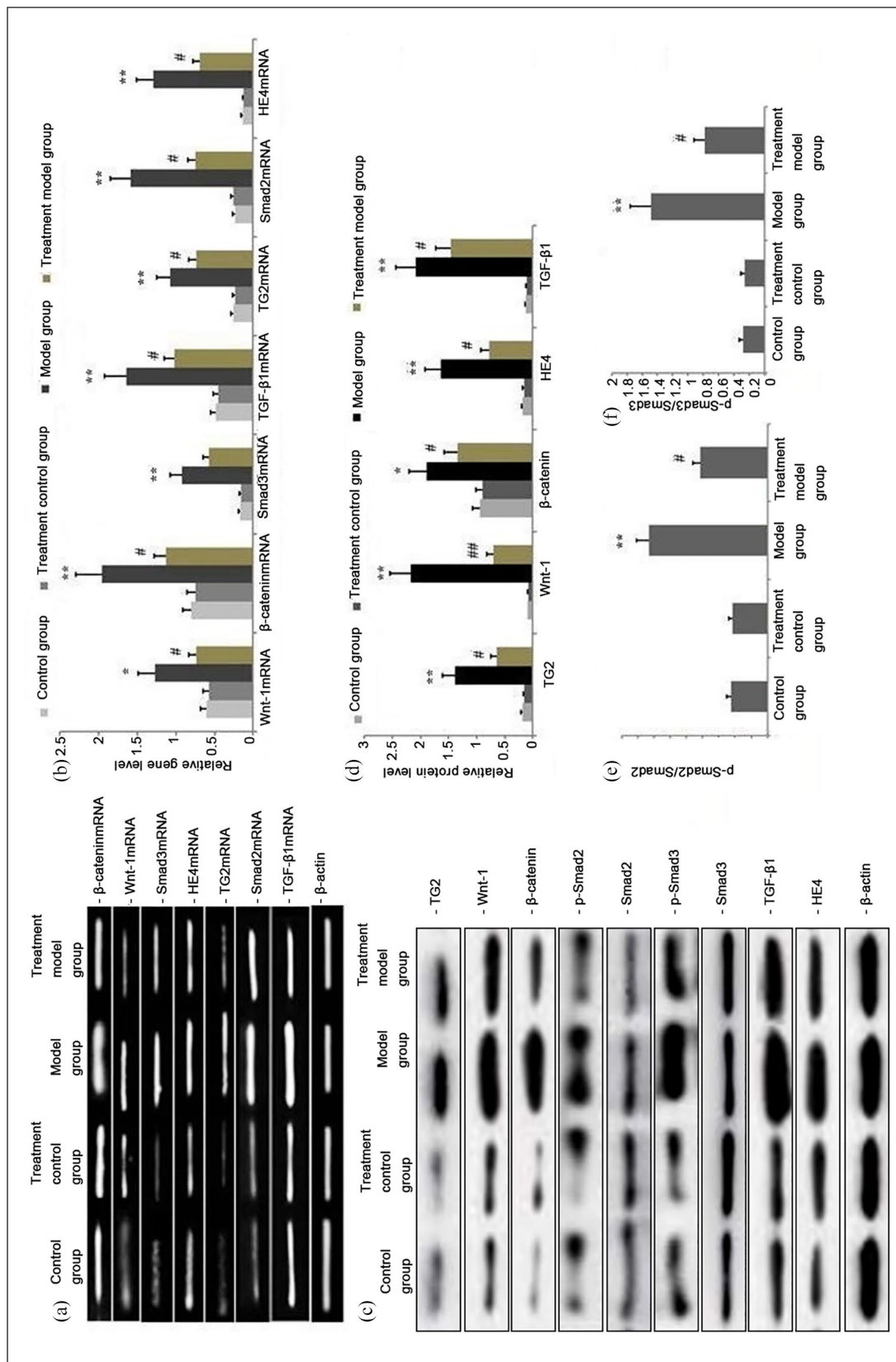
$P > 0.05$ the control mice versus the control treatment group.

Figure 6. Effects of XBJ treatment on TG2, Wnt-1, β-catenin, Smad2, Smad3, HE4, and TGF-β1 gene and protein expressions. (a) and (b) The mice in the model and treatment groups were exposed to PQ. (c)–(e) The gene expression levels of TG2, Wnt-1, β-catenin, HE4, Smad3, and TGF-β1 were measured by qRT-PCR. The expression levels of proteins TG2, Wnt-1, β-catenin, HE4, p-Smad2, p-Smad3, and TGF-β1 were measured by Western blot analysis. Quantitative densitometry data obtained from three independent experiments are presented as mean ± SD.
*$p < 0.05$ versus the control group.
#$P < 0.05$ versus the model group.
$P > 0.05$ the control mice versus the control treatment group.

XBJ administration blocked TG2, HE4, and α-SMA activity in PQ-exposed mouse lungs

XBJ delivery has anti-fibrotic and anti-inflammatory effects on fibrosis and peripheral inflammation. These effects are due to the inhibition of different pro-inflammatory and pro-fibrotic signaling molecules, such as HE4, α-SMA, and TG2. The immunohistochemical results showed that HE4, α-SMA, and TG2 were strongly expressed in the lungs of the mice exposed to PQ (Figure 7). Nevertheless, XBJ delivery markedly halted PQ-induced HE4, α-SMA, and TG2 activities. However, no difference was found between the control and the control treatment groups.

XBJ impeded the protein levels of α-SMA, MMP-9, CTGF, collagen-I, and collagen-III in mice with PQ-induced pulmonary fibrosis

MMP-9, α-SMA, CTGF, collagen-I, and collagen-III protein levels were quantified by Western blot analysis in pulmonary tissues of mice to examine the effects of XBJ on the levels of α-SMA, CTGF, MMP-9, collagen-I, and collagen-III protein expressions in mice with PQ-induced pulmonary fibrosis. The model group had higher MMP-9, CTGF, α-SMA, collagen-I, and collagen-III levels than the control group ($P < 0.05$; Figure 8(a)–(d)). XBJ halted the elevation in MMP-9, α-SMA, collagen-I, and collagen-III protein levels. However, no difference was found between the control and the control treatment groups.

XBJ decreased CTGF, HE4, TGF-β1, and MMP-9 levels in BAL

CTGF, HE4, TGF-β1, and MMP-9 are the key proteins in the induction of pulmonary fibrosis. The levels of these proteins in the BAL were quantified to determine the effects of XBJ on TGF-β1, HE4, CTGF, and MMP-9. Chronic exposure to PQ produced a significant elevation in BAL levels of TGF-β1, HE4, CTGF, and MMP-9 (Figure 8(e)–(g)). XBJ significantly decreased the levels of TGF-β1, HE4, CTGF, and MMP-9 in BAL in the mice exposed to PQ. However, no difference was found between the control and the control treatment groups.

XBJ decreased HE4, LN, and HA expression in mice exposed to PQ

HE4, LN, and HA levels in plasma were quantified via ELISA to establish the effects of XBJ on HE4, LN, and HA expression in mice exposed to PQ. In contrast to the control group, the group exposed to PQ had higher protein levels of HE4, LN, and HA in plasma (Figure 8(h) and (i)). XBJ halted the elevation in HA and LN protein levels. However, no difference was found between the control and the control treatment groups.

XBJ diminished pulmonary fibrosis induced by PQ

The effects of XBJ on PQ-induced pulmonary fibrosis were determined. The alveolar septa were significantly thickened, and collagen was deposited in the lungs of the mice 14 days after exposure to PQ according to H&E staining and Masson's trichrome staining. In contrast to the degree of pulmonary fibrosis of mice exposed to PQ, XBJ-treated mice were significantly decreased at 14 days (Figure 9). However, the control and the control treatment groups did not differ.

The degree of pulmonary fibrosis was scored, and collagen deposition was evaluated by quantifying the Hyp content in the lungs. The fibrotic lesion scores and Hyp content were significantly increased in the saline-treated control mice 14 days after PQ delivery than in the PQ-treated mice. The fibrotic lesion scores and Hyp content in XBJ-treated mice were significantly lower than in the untreated PQ-exposed mice (Figure 9). However, the control and the control treatment groups did not differ.

Discussion

miRNA expression was profiled through high-throughput genomic approaches to gain insight into the diagnosis, classification, pathogenesis, prognosis, and stratification of human diseases, including tissue fibrosis.[38,39] These approaches were successfully used to study IPF; miR-21 and let-7d are important contributors to the development of lung fibrosis.[12,33–35,40] miR-140-5p overexpression inhibited lipopolysaccharide-induced human intervertebral disk inflammation and degeneration by downregulating toll-like receptor 4.[41] Upregulated miR-140-5p could protect synovial injury by restraining inflammation reaction and apoptosis of synoviocytes in knee osteoarthritis (KOA) rats via the TLR4/Myd88/NF-κB signaling pathway.[42] miR-140 knockout primary lung fibroblasts have a higher myofibroblast percentage compared with wild-type primary lung fibroblasts;
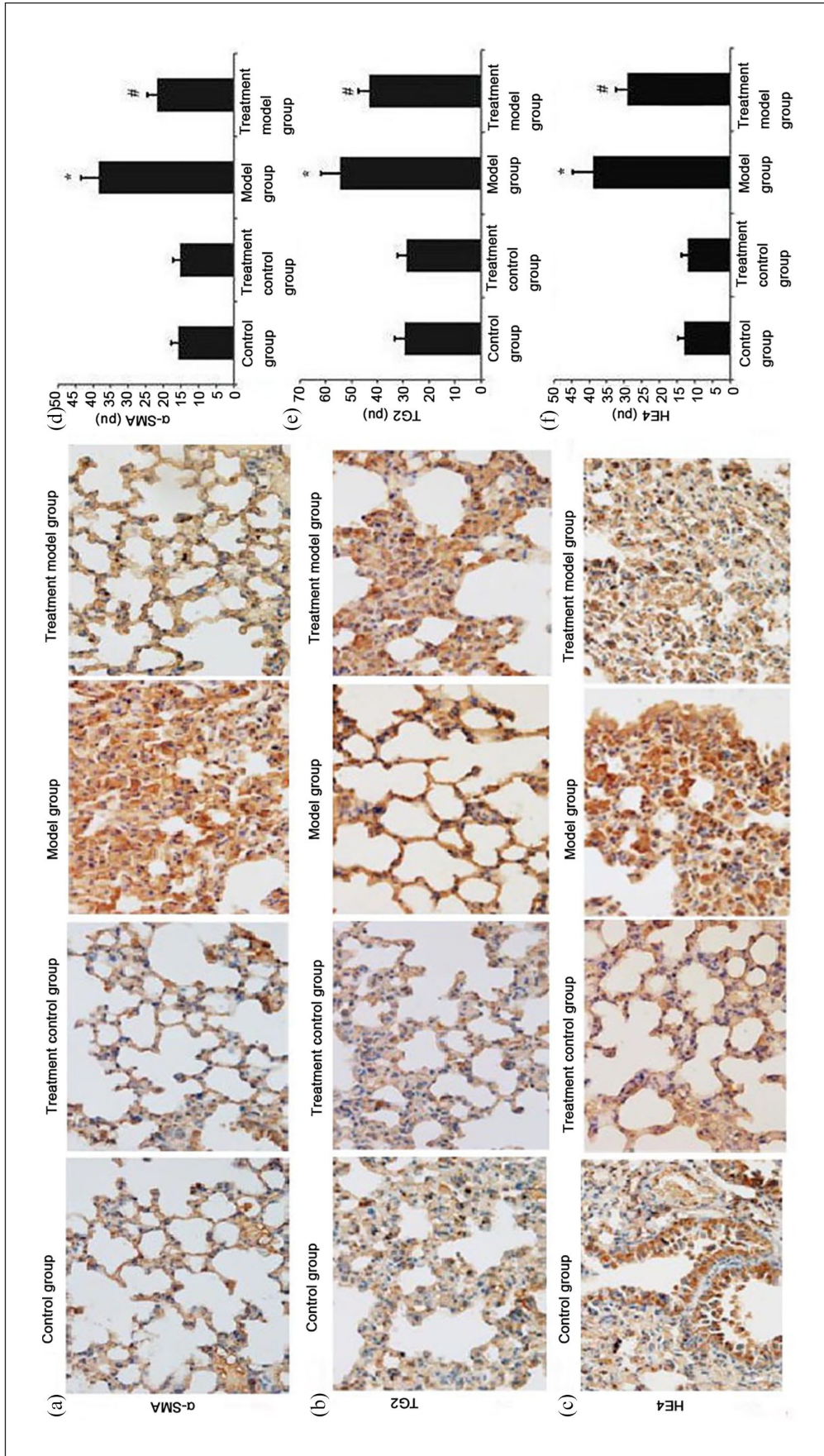
Figure 7. Effects of XBJ on HE4, TG2, and α-SMA activities in the lungs of a PQ-exposed mouse. Immunohistochemistry was used to measure HE4, TG2, and α-SMA activities in mice exposed to PQ. (a) Representative immunostaining patterns for HE4, TG2, and α-SMA. (b)–(d) Statistical summary of the densitometric analyses of HE4, TG2, and α-SMA staining is presented as mean ± SD.

*$p < 0.05$ versus the control mice.

#$P < 0.05$ versus the model group.
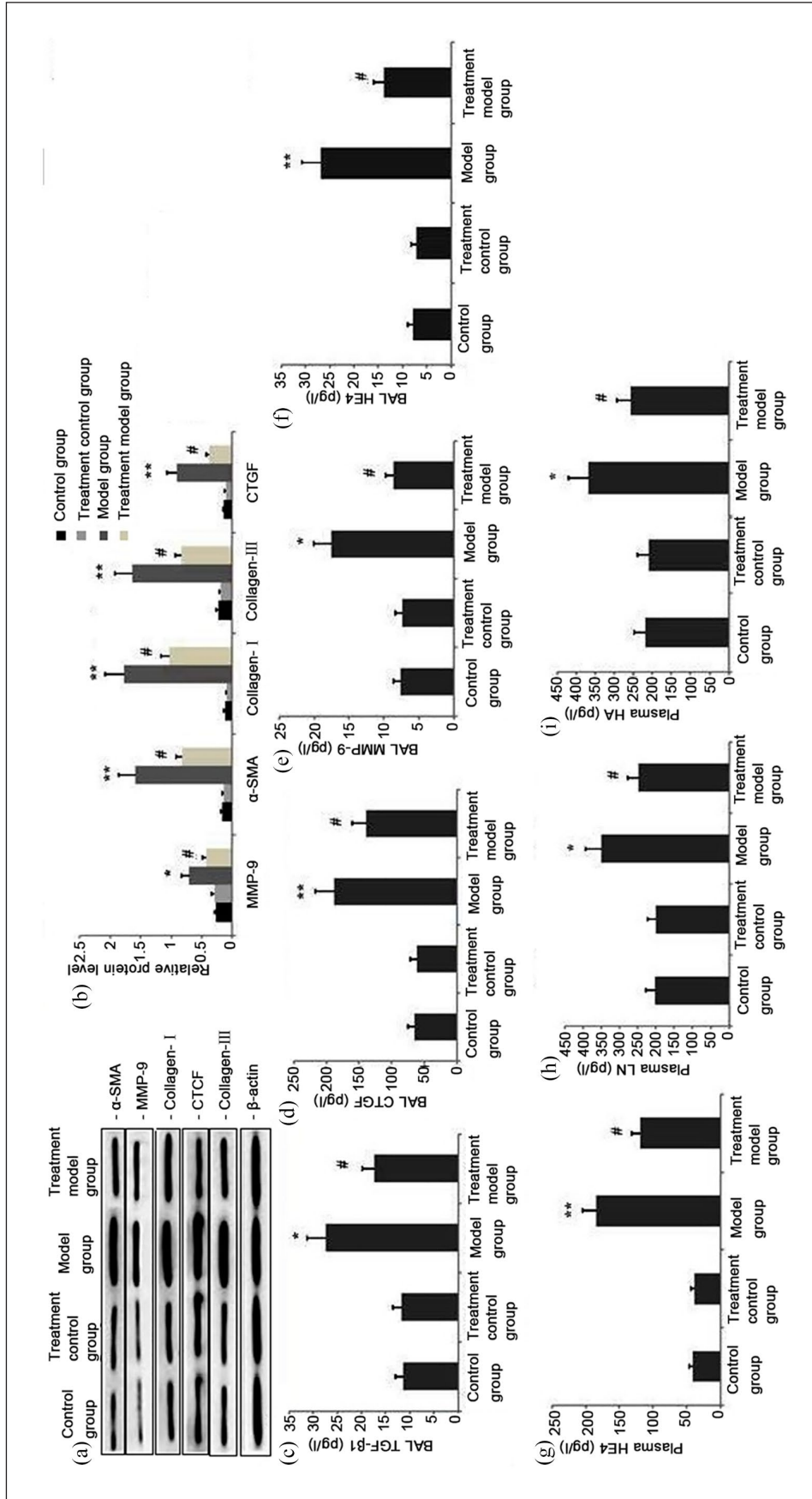
$P > 0.05$ the control mice versus the control treatment group.

Figure 8. Effects of XBJ on the expression levels of lung MMP-9, α-SMA, collagen-I, and collagen-III proteins; BAL TGF-βI, CTGF, MMP-9, α-SMA, collagen-I, and collagen-III proteins; BAL TGF-βI, and HA levels. The mice were exposed to ((a) and (b)) PQ, and MMP-9, α-SMA, collagen-I, and collagen-III protein levels were measured by Western blot analysis; (c) BAL TGF-βI, (d) CTGF, (e) MMP-9, and (f) HE4 levels and plasma (g) HE4, (h) LN, and (i) HA were quantified by ELISA. Quantitative densitometry data were obtained from three independent experiments and presented as mean ± SD.

*$*P < 0.05$ versus the control group.

$\#P < 0.05$ versus the model group.

$P > 0.05$ the control mice versus the control treatment group.

the loss of miR-140 expression leads to increased activation of TGF-β1 signaling and increased myofibroblast differentiation.[13] miR-140-5p negatively regulates Wnt1, autophagic flux, and tumorigenic potential expression.[43] In this study, miR-140-5p mimics were successfully transfected into A549 cells for 24 h (Figure 1). The elevated miR-140-5p levels in A549 cells significantly decreased Wnt1, β-catenin, p-Smad3, and TGF-β1 expressions ($P < 0.05$). Thus, miR-140-5p could block the Smad/TGF-β1 and the Wnt1/β-catenin fibrogenic signaling pathways.

In a previous study,[11] we evaluated the miRNAs involved in the differential susceptibility of two mouse strains to PQ-induced lung fibrosis. In this work, miR-140-5p expression was the most statistically significant (Figures 1 and 2). A definite correlation with PQ-induced lung fibrosis progression was determined. The change in miR-140-5p expression indicated a main pathogenic mechanism in the development of lung fibrosis instead of a secondary effect of the disease. We initially concluded that miR-140-5p expression was reduced in progressive lung fibrosis (Figures 2 and 3). Furthermore, compared with the controls, the samples with overexpressed miR-140-5p showed improvement (Figure 2). The considerable increase in miR-140-5p halted the activity of the Smad/TGF-β1 and Wnt1/β-catenin fibrogenic signaling pathway in mouse lung tissue (Figure 3). This result indicated a marked reduction in inflammatory cell infiltration and collagen deposition and in diminished PQ-induced lung fibrosis (Figure 2). miR-140-5p is a fibrosis-related gene and might be crucial in the pathogenesis of pulmonary fibrosis by regulating the Wnt1/β-catenin fibrogenic signaling pathway.

A beneficial feedback regulatory loop in the Wnt/β-catenin and miR-140-5p signaling pathway can maintain the "stemness" of cerebral protection of dexmedetomidine against hypoxic-ischemic brain damage. miR-140-5p and Wnt/β-catenin ease the stemness by targeting downstream genes in the regulatory loop.[44] In this evaluation, miR-140-5p was reduced, the canonical WNT/β-catenin signaling pathway was activated, and the pulmonary fibrosis with PQ exposure was aggravated (Figures 1–3). Target Scan was used to determine possible miR-140-5p targets. Wild-type and mutant Wnt1 were constructed for a dual-luciferase reporter assay to validate the interaction between miR-140-5p and Wnt1. Wnt1 is a direct target of miR-140-5p (Figure 4(a)–(f)). miR-140-5p inhibited pulmonary fibrosis by blocking the activity of the Wnt1/β-catenin signaling pathway.

Activation of the canonical Wnt/β-catenin signaling pathway is connected to fibrosis, fibroblast activation, and tissue repair.[45] β-catenin is a pivotal part of the canonical Wnt signaling pathway and functions as a gene transcription activator.[45] Cytosolic β-catenin is stabilized with Wnt ligands and permits the latter to function as a transcriptional co-activator. Numerous growth factors, including TGF-β, stimulate β-catenin signaling immediately or by generating the autocrine Wnt ligand.[46] Stabilized, that is, unphosphorylated, β-catenin stimulates several target genes, including growth factors, extracellular matrix (ECM) proteins, MMPs, and pro-inflammatory mediators and enzymes.[29] The part of β-catenin signaling in the induction of the EMT has been established. Furthermore, the Wnt/β-catenin axis is involved in IPF development.[28,29–31] In our evaluation, PQ-exposed mice lung tissue had low miR-140-5p expression and high gene and protein expression levels of β-catenin, Wnt-1, α-SMA, CTGF, and Col-I, as well as aggravated pulmonary fibrosis (Figures 2 and 3). Wnt/β-catenin pathway inhibition mitigated and reversed pulmonary fibrosis in a mouse model of PQ-induced pulmonary fibrosis by upregulating miR-140-5p expression (Figures 2 and 3). The treatment with XBJ upregulated miR-140-5p expression, blocked the Wnt/β-catenin pathway, and improved and reversed pulmonary fibrosis in a mouse model of PQ-induced pulmonary fibrosis (Figures 5, 6, and 9)

TG2 plays important roles in normal fibroblast activity in vitro. TG2 knockdown causes the defects in fibroblast function, including contraction and migration. TG2 may promote tissue fibrosis through several ways. TG2 may allow fibronectin to cross-link with extracellular collagen, thereby contributing to the resistance of collagen to degradation.[47] TG2 also enhances fibrillar fibronectin production and maturation in an enzyme-independent manner.[48–50] TG2 is upregulated in PQ-induced lung fibrosis mouse models and promotes fibrosis by increasing MMP levels and Smad2, Smad3, TGF-β1, and β-catenin phosphorylation. However, XBJ treatment downregulated TG2 expression; decreased MMP; phosphorylated Smad2, Smad3, TGF-β1, and β-catenin levels; and ameliorated pulmonary fibrosis (Figure 8). Therefore, XBJ-induced TG2 inhibition reduced PQ-induced lung fibrosis.
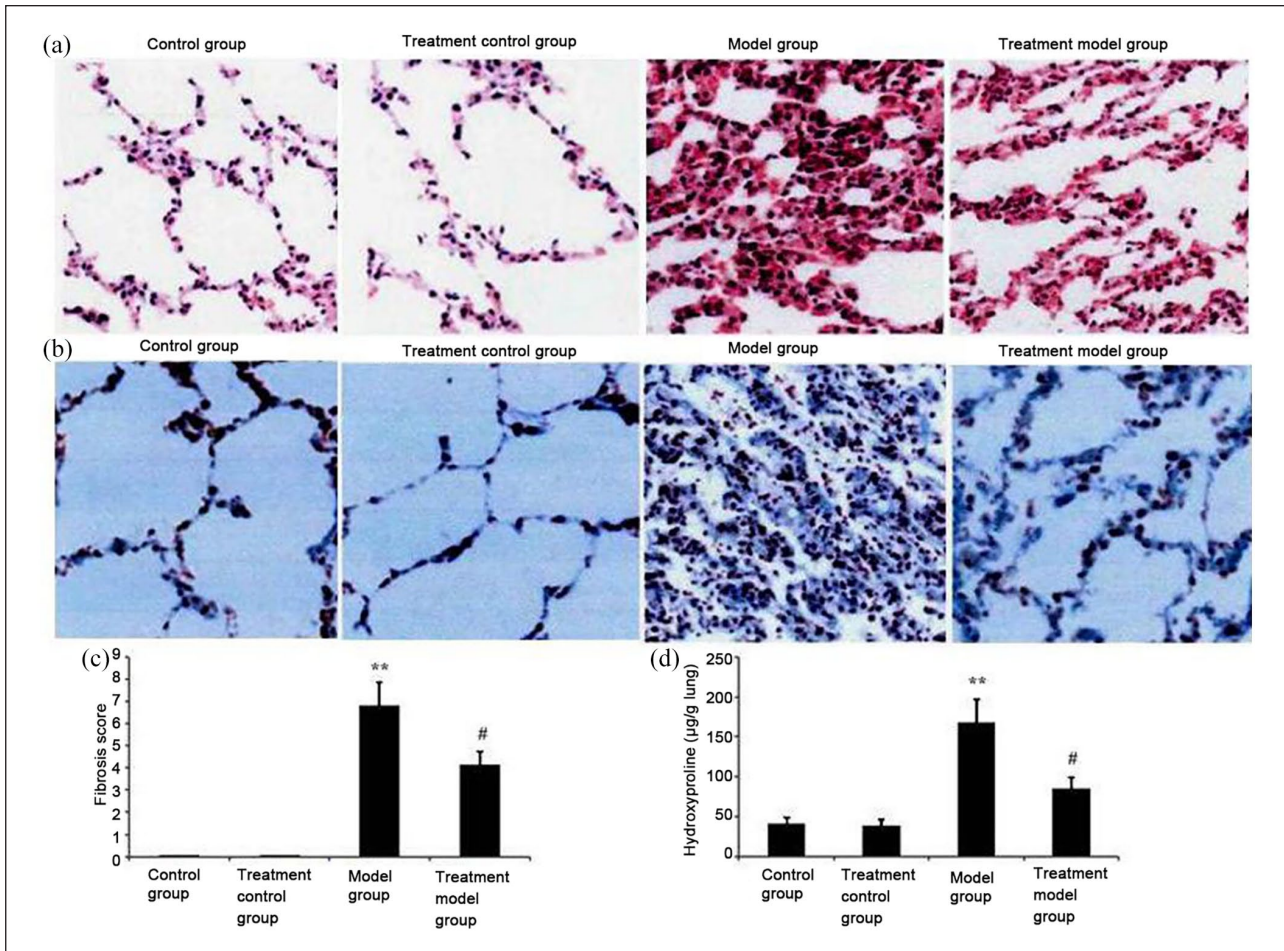
Figure 9. Histopathological changes in the lungs of mice. (a) and (b) Histopathological changes in the lung tissues of mice. (a) a → c, H&E staining, 200× magnification and (b) a → c, Masson's trichrome staining, 200× magnification. (c) Statistical results on pulmonary fibrosis in mice. Pulmonary fibrosis scores and hydroxyproline levels from three separate experiments are expressed as the mean ± SD.
**P < 0.01 versus the control group;
#P < 0.05 versus the model group.
P > 0.05 the control mice versus the control treatment group.

MMPs play important roles in cell infiltration, tissue remodeling, and fibrosis. Among many MMPs, MMP-9 can increase pulmonary fibrosis activity in several pulmonary diseases.[51,52] In this study, XBJ inhibited MMP-9 expression by upregulating miR-140-5p and attenuating pulmonary fibrosis (Figure 8).

Most genes targeted by TGF-β are transcriptionally regulated in a Smad3-dependent manner.[53–55] Human and animal model studies indicated that TGF-β1 can increase CTGF and α-SMA expression, which was upregulated in fibrosis, thereby stimulating fibroblasts to synthesize ECM proteins and playing a critical role in fibrotic disease progression.[56] Consistent with these observations, α-SMA, TGF-β1, and CTGF in PQ-exposed mice

treated with XBJ were significantly inhibited by blocking Smad2 and/or Smad3 activity (Figures 7, 8, and 9).

LNs are ECM proteins with high-molecular weights.[57] These proteins are key components of the basal lamina, including the basement membrane, and act as the foundation of most cells and organs.[57] HA is also a key component of the ECM in cell proliferation and migration. It may participate in the progression of pulmonary fibrosis and some malignant tumors.[58] XBJ injection suppressed the increase in laminin and HA after PQ treatment, thereby mitigating PQ-induced pulmonary fibrosis (Figure 8(h) and (i)).

Previous studies reported the high HE4 expression in lung biopsy samples from patients with
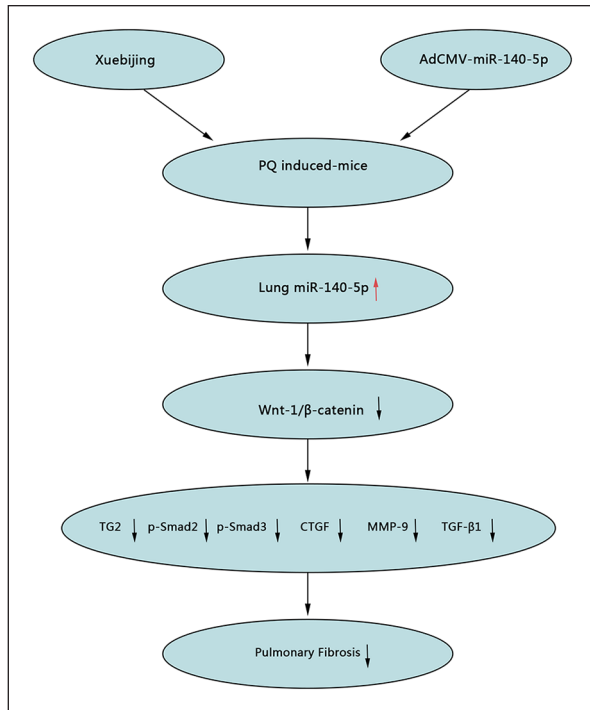
Figure 10. Potential unifying mechanism for the anti-fibrotic effects of XBJ.

cystic fibrosis (CF).[59] Moreover, HE4 serum levels are positively correlated with the overall severity of CF and the degree of pulmonary dysfunction.[59] In this experiment, lung tissue HE4 gene and protein levels were significantly elevated in PQ-induced pulmonary fibrosis mice (Figures 6(a)–(d) and 7(c)). Further studies showed that HE4 levels in plasma and BAL obviously increased (Figure 8(f) and (g)). However, treatment with XBJ injection significantly decreased the gene and protein levels of HE4 in lung tissues (Figures 6(a)–(d) and 7(c)), in plasma, and in BAL (Figure 8(f) and (g)). Thus, HE4 can be used as a marker for PQ-induced pulmonary fibrosis.

Animal models of PQ-induced lung fibrosis and injury have been used to examine the pathogenesis of pulmonary fibrosis and injury and the therapeutic potential of various agents.[30,60,61] In our evaluation, H&E staining of lung sections showed that intraperitoneal injection of PQ caused damage to the normal pulmonary architecture, infiltration of inflammatory cells, significant proliferation of fibroblasts, and remarkable deposition of fibrillar collagen (Figure 9). The pathological alterations were substantially improved following the administration of XBJ. Significantly less deposition of collagen fibers was noted following XBJ delivery, as indicated by Masson's trichrome staining

(Figure 9). The pulmonary levels of Hyp, a key component of collagen, were quantified in five mice subjected to various experimental conditions to establish the severity of pulmonary fibrosis. Hyp levels decreased after XBJ treatment (Figure 9). This result indicates the protective role of XBJ by counteracting ECM accumulation. Moreover, the expression levels of the potent pro-fibrotic factors (TGF-β1, CTGF, MMP-9, collagen-I, and collagen-III) in the PQ-exposed mice were markedly decreased following treatment with XBJ compared with PQ-exposed mice that did not receive XBJ (Figure 8). These in vivo outcomes showed that the protective effects of XBJ against pulmonary fibrosis were primarily reflected in the anti-fibrotic effect. In our in vivo evaluation, a PQ-induced lung fibrosis mouse model was utilized to examine the effects of XBJ on PQ toxicity.

Intravenous XBJ therapy is highly efficient in the treatment of endotoxin-induced tissue injury and in halting the uncontrolled release of endogenous inflammatory mediators from endotoxin-stimulated mononuclear macrophages.[62] Intravenous XBJ therapy inhibits procollagen mRNA expression, decreases lipid peroxidation, increases superoxide dismutase activity, reduces fibroblast generation, and inhibits ECM sedimentation, thereby reducing TGF-β1 expression.[24] This evaluation offered insights into the potential mechanisms of the Wnt-1/β-catenin signaling pathway and TG2 repression by XBJ. XBJ elevates miR-140-5p expression and halts alveolar fibroblast activation and EMT and ECM production. Finally, XBJ improves pulmonary fibrosis. These outcomes suggested the key role of XBJ in preventing the occurrence of pulmonary fibrosis and its protective effects after PQ exposure.

Conclusion

XBJ administration significantly attenuated PQ-induced pulmonary fibrosis by blocking and reducing the accumulation of collagenous fiber in PQ-treated mice. Furthermore, in vitro and in vivo evaluations indicated that the protective effects of XBJ against pulmonary fibrosis were achieved by upregulating miR-140-5p expression. Such effects are related to the modulation of pro-fibrotic gene expression and fibroblasts, such as the repression of the TG2 and the Wnt-1/β-catenin signaling pathway activities (Figure 10). The positive effects of the in vivo delivery of XBJ on pulmonary fibrosis

detailed support a possible novel therapeutic technique for treating PQ-induced pulmonary fibrosis and other types of pulmonary fibrosis. Therefore, the mechanisms underlying XBJ activity must be further explored through pharmacological evaluation, and its potential in preventing and treating pulmonary fibrosis must be assessed.

This study has some limitations. TG2 expression and the Wnt-1/β-catenin signaling pathway were hindered by the elevated expression of miR-140-5p. miR-140-5p may be involved in pulmonary fibrosis, and further research is needed. XBJ has a certain effect on patients with pulmonary fibrosis caused by PQ poisoning.[63] This experiment revealed the molecular mechanisms through which XBJ resists PQ-induced pulmonary fibrosis. However, the anti-fibrosis effect of XBJ may involve inflammation, oxidation, and autophagy. Thus, its mechanism requires further study. This experiment does not involve the study of the long-term prognosis and adverse reactions of pulmonary fibrosis treatment using XBJ. There are many active ingredients in XBJ injection. This experiment cannot determine the effect of each active ingredient of XBJ injection on pulmonary fibrosis. Further research is necessary.

Animal welfare

This study followed the international, national, and/or institutional guidelines for humane animal treatment and complied with relevant legislation. All experiments were carried out according to the National Institutes of Health Guidelines for the Care and Use of Laboratory Animals, and all animals were treated in strict accordance with protocols approved by the Institutional Animal Care and Use Committee of Kunming Medical University. All applicable international, national, and/or institutional guidelines for the care and use of animals were followed.

Declaration of conflicting interests

The author(s) declared no potential conflicts of interest with respect to the research, authorship, and/or publication of this article.

Ethical approval

All animal experiments were approved by the Animal Experimental Ethics Committee of Kunming Medical University (Approval No. KYYM-2018-012-E23)

Funding

ORCID iD

Ming-wei Liu https://orcid.org/0000-0002-3728-2350

References

1. Li C, Hu D, Xue W, et al. (2018) Treatment outcome of combined continuous venovenous hemofiltration and hemoperfusion in acute paraquat poisoning: A prospective controlled trial. *Critical Care Medicine* 46(1): 100–107.

2. Weerasinghe M, Konradsen F, Eddleston M, et al. (2018) Vendor-based restrictions on pesticide sales to prevent pesticide self-poisoning—A pilot study. *BMC Public Health* 18(1): 272.

3. Buckley NA, Karalliedde L, Dawson A, et al. (2004) Where is the evidence for treatments used in pesticide poisoning? Is clinical toxicology fiddling while the developing world burns? *Journal of Toxicology-Clinical Toxicology* 4: 113–116.

4. Jiang Y, Yang W and Gui S (2018) Procyanidin B2 protects rats from paraquat-induced acute lung injury by inhibiting NLRP3 inflammasome activation. *Immunobiology* 223(10): 555–561.

5. Manuel C, Gunnell DJ, van der Hoek W, et al. (2008) Self-poisoning in rural Sri Lanka: Small-area variations in incidence. *BMC Public Health* 8: 26.

6. Min YG, Ahn JH, Chan YC, et al. (2011) Prediction of prognosis in acute paraquat poisoning using severity scoring system in emergency department. *Clinical Toxicology* 49(9): 840–845.

7. Bartel DP (2000) MicroRNAs: Target recognition and regulatory functions. *Cell* 136: 215–233.

8. Mukhadi S, Hull R, Mbita Z, et al. (2015) The role of MicroRNAs in kidney disease. *Non Coding RNA* 1(3): 192–221.

9. Sand M, Gambichler T, Sand D, et al. (2009) MicroRNAs and the skin: Tiny players in the body's largest organ. *Journal of Dermatological Science* 53(3): 169–175.

10. Zhao X, Wang K, Liao Y, et al. (2015) MicroRNA-101a inhibits cardiac fibrosis induced by hypoxia via targeting TGFβRI on cardiac fibroblasts. *Cellular Physiology and Biochemistry* 35: 213–226.

11. Wu J, Liu S, Yuan ZW, et al. (2018) MicroRNA-27a suppresses detrusor fibrosis in streptozotocin-induced diabetic rats by targeting PRKAA2 through the TGF-β1/Smad3 signaling pathway. *Cellular Physiology and Biochemistry* 45: 1333–1349.

12. Liu MW, Liu R, Wu HY, et al. (2016) *Radix puerariae* extracts ameliorate paraquat-induced pulmonary fibrosis by attenuating follistatin-like 1 and nuclear

factor erythroid 2p45-related factor-2 signalling pathways through downregulation of miRNA-21 expression. *BMC Complementary and Alternative Medicine* 16: 11.

13. Duru N, Zhang Y, Gernapudi R, et al. (2016) Loss of miR-140 is a key risk factor for radiation-induced lung fibrosis through reprogramming fibroblasts and macrophages. *Scientific Reports* 6: 39572.

14. Wang C, Song X, Li Y, et al. (2013). Low-dose paclitaxel ameliorates pulmonary fibrosis by suppressing TGF-beta1/Smad3 pathway via miR-140 upregulation. *PLoS ONE* 8(8): e70725.

15. Olsen KC, Epa AP, Kulkarni AA, et al. (2014) Inhibition of transglutaminase 2, a novel target for pulmonary fibrosis, by two small electrophilic molecules. *American Journal of Respiratory Cell and Molecular Biology* 50(4): 737–747.

16. Poole Pant A, Baker KS, Kopec AK, et al. (2019) Chronic liver injury drives non-traditional intrahepatic fibrin(ogen) crosslinking via tissue transglutaminase. *Journal of Thrombosis and Haemostasis* 17(1): 113–125.

17. Liu Y, Li Y, Xu Q, et al. (2018) Long non-coding RNA-ATB promotes EMT during silica-induced pulmonary fibrosis by competitively binding miR-200c. *Biochimica Et Biophysica Acta. Molecular Basis of Disease* 1864(2): 420–431.

18. Xu J, Lamouille S and Derynck R (2009) TGF-beta-induced epithelial to mesenchymal transition. *Cell Research* 19: 156–172.

19. Jia P, Wang S, Meng X, et al. (2013) Effects of ionic liquid and nanogold particles on high-performance liquid chromatography-electrochemical detection and their application in highly efficient separation and sensitive analysis of five phenolic acids in Xuebijing injection. *Talanta* 107: 103–110.

20. Jiang M, Zhou M, Han Y, et al. (2014) Identification of NF-κB inhibitors in Xuebijing injection for sepsis treatment based on bioactivity-integrated UPLC-Q/TOF. *Journal of Ethnopharmacology* 147: 426–433.

21. Liu MW, Su MX, Zhang W, et al. (2014) Protective effect of Xuebijing injection on paraquat-induced pulmonary injury via down-regulating the expression of p38 MAPK in rats. *BMC Complementary and Alternative Medicine* 14: 498.

22. Wang L, Xu Q, Huang S, et al. (2014) Effects of methylprednisolone plus Xuebijing on bleomycin-induced acute exacerbation of pulmonary fibrosis in rats. *Zhonghua Yi Xue Za Zhi* 94(4): 301–305.

23. Zhang BL, Li ZJ, Song LY, et al. (2008) Study on renoprotective effect of Xuebijing and Rosiglitazone in rats with focal segmental glomerular fibrosis. *Chinese Critical Care Medicine* [*Zhongguo Wei Zhong Bing Ji Jiu Yi Xue*] 20(5): 299–300.

24. Zheng X, Sun X, Ma P, et al. (2012) Therapeutic potential of intravenous Xuebijing on transforming growth factor beta1 and procollagen type III peptide in patients with acute paraquat poisoning. *Journal of Traditional Chinese Medicine* [*Chung I Tsa Chih Ying Wen Pan*] 32(4): 584–589.

25. Chen X, Shi C, Cao H, et al. (2018) The hedgehog and Wnt/β-catenin system machinery mediate myofibroblast differentiation of LR-MSCs in pulmonary fibrogenesis. *Cell Death & Disease* 9: 639.

26. Qi J, Lee J, Saquet A, et al. (2017) Autoinhibition of dishevelled protein regulated by its extreme C terminus plays a distinct role in Wnt/β-catenin and Wnt/planar cell polarity (PCP) signaling pathways. *Journal of Biological Chemistry* 292: 5898–5908.

27. Zhu Y, Wang J, Meng X, et al. (2017) A positive feedback loop promotes HIF-1α stability through miR-210-mediated suppression of RUNX3 in paraquat-induced EMT. *Journal of Cellular and Molecular Medicine* 21: 3529–3539.

28. DiRocco DP, Kobayashi A, Taketo MM, et al. (2017) Wnt4/β-catenin signaling in medullary kidney myofibroblasts. *Journal of the American Society of Nephrology* 24: 1399–1412.

29. Aumiller V, Balsara N, Wilhelm J, et al. (2013) WNT/β-catenin signaling induces IL-1β expression by alveolar epithelial cells in pulmonary fibrosis. *American Journal of Respiratory Cell and Molecular Biology* 49: 96–104.

30. Tanjore H, Degryse AL, Crossno PF, et al. (2013) β-catenin in the alveolar epithelium protects from lung fibrosis after intratracheal bleomycin. *American Journal of Respiratory and Critical Care Medicine* 187(6): 630–639.

31. Yang Z, Ji L, Jiang G, et al. (2018) FL118, a novel camptothecin analogue, suppressed migration and invasion of human breast cancer cells by inhibiting epithelial-mesenchymal transition via the Wnt/β-catenin signaling pathway. *Bioscience Trends* 12: 40–46.

32. Cheung WY, Hovey O, Gobin JM, et al. (2018) Efficient nonviral transfection of human bone marrow mesenchymal stromal cells shown using placental growth factor overexpression. *Stem Cells International* 2018: 1310904.

33. Schapochnik A, da Silva MR, Leal MP, et al. (2018) Vitamin D treatment abrogates the inflammatory response in paraquat-induced lung fibrosis. *Toxicology and Applied Pharmacology* 355: 60–67.

34. Spronk HM, Soute BA, Schurgers LJ, et al. (2003) Tissue-specific utilization of menaquinone-4 results in the prevention of arterial calcification in warfarin-treated rats. *Journal of Vascular Research* 40(6): 531–537.

35. Kim MR, Kwon K, Jung YK, et al. (2018) A rapid real-time PCR method to differentiate between mottled

skate (*Beringraja pulchra*) and other skate and ray species. *Food Chemistry* 255: 112–119.

36. Kivirikko KI, Laitinen O and Prockop DJ (1967) Modification of a specific assay for hydroxyproline in urine. *Analytical Biochemistry* 19: 249–255.

37. Ashcroft T, Simpson JM and Timbrell V (1998) Simple method of estimating severity of pulmonary fibrosis on a numerical scale. *Journal of Clinical Pathology* 41: 467–470.

38. Ebrahimi A and Sadroddiny E (2015) MicroRNAs in lung diseases: Recent findings and their pathophysiological implications. *Pulmonary Pharmacology & Therapeutics* 34: 55–63.

39. Saco TV, Parthasarathy PT, Cho Y, et al. (2015) Micro RNAs: The future of idiopathic pulmonary fibrosis therapy. *Cell Biochemistry and Biophysics* 71(1): 509–511.

40. Ramos-Vara JA and Miller MA (2014) When tissue antigens and antibodies get along: Revisiting the technical aspects of immunohistochemistry—The red, brown, and blue technique. *Veterinary Pathology* 51(1): 42–87.

41. Huang X, Qiao F and Xue P (2019) The protective role of microRNA-140-5p in synovial injury of rats with knee osteoarthritis via inactivating the TLR4/Myd88/NF-κB signaling pathway. *Cell Cycle* 18: 2344–2358.

42. Zhang Q, Weng Y, Jiang Y, et al. (2018) Overexpression of miR-140-5p inhibits lipopolysaccharide-induced human intervertebral disc inflammation and degeneration by downregulating toll-like receptor 4. *Oncology Reports* 40(2): 793–802.

43. Yeon M, Lee S, Lee JE, et al. (2019) CAGE-miR-140-5p-Wnt1 axis regulates autophagic flux, tumorigenic potential of mouse colon cancer cells and cellular interactions mediated by exosomes. *Frontiers in Oncology* 9: 1240.

44. Han XR, Wen X, Wang YJ, et al. (2018) MicroRNA-140-5p elevates cerebral protection of dexmedetomidine against hypoxic-ischaemic brain damage via the Wnt/β-catenin signalling pathway. *Journal of Cellular and Molecular Medicine* 22: 3167–3182.

45. Ge WS, Wang YJ, Wu JX, et al. (2014) β-catenin is overexpressed in hepatic fibrosis and blockage of Wnt/β-catenin signaling inhibits hepatic stellate cell activation. *Molecular Medicine Reports* 9: 2145–2151.

46. Rims CR and McGuire JK (2014) Matrilysin (MMP-7) catalytic activity regulates β-catenin localization and signaling activation in lung epithelial cells. *Experimental Lung Research* 40: 126–136.

47. Tovar-Vidales T, Roque R, Clark AF, et al. (2008) Tissue transglutaminase expression and activity in normal and glaucomatous human trabecular meshwork cells and tissues. *Investigative Ophthalmology & Visual Science* 49(2): 622–628.

48. Kang Oh SC, Min BW and Lee DH (2018) Transglutaminase 2 regulates self-renewal and stem cell marker of human colorectal cancer stem cells. *Anticancer Research* 38(2): 787–794.

49. Tatsukawa H, Otsu R, Tani Y, et al. (2018) Isozyme-specific comprehensive characterization of transglutaminase-crosslinked substrates in kidney fibrosis. *Scientific Reports* 8(1): 7306.

50. Tovar-Vidales T, Clark AF and Wordinger RJ (2011) Focus on molecules: Transglutaminase 2. *Experimental Eye Research* 93(1): 2–3.

51. Tang H, Mao J, Gao L, et al. (2013) Effect of anti-sense TIMP-1 cDNA on the expression of TIMP-1 and MMP-2 in lung tissue with pulmonary fibrosis induced by bleomycin. *Molecular Medicine Reports* 7(1): 149–153.

52. Du X, Shimizu A, Masuda Y, et al. (2012) Involvement of matrix metalloproteinase-2 in the development of renal interstitial fibrosis in mouse obstructive nephropathy. *Laboratory Investigation* 92(8): 1149–1160.

53. Choi J, Park SJ, Jo EJ, et al. (2013) Hydrogen peroxide inhibits transforming growth factor-β1-induced cell cycle arrest by promoting Smad3 linker phosphorylation through activation of Akt-ERK1/2-linked signaling pathway. *Biochemical and Biophysical Research Communications* 435: 634–639.

54. Dahle O and Kuehn MR (2013) Polycomb determines responses to smad2/3 signaling in embryonic stem cell differentiation and in reprogramming. *Stem Cells* 31(8): 1488–1497.

55. Cho JW, Il J and Lee KS (2013) Downregulation of type I collagen expression in silibinin-treated human skin fibroblasts by blocking the activation of Smad2/3-dependent signaling pathways: Potential therapeutic use in the chemoprevention of keloids. *International Journal of Molecular Medicine* 31(5): 1148–1152.

56. Chen Y, Lebrun JJ and Vale W (1996) Regulation of transforming growth factor beta- and activin-induced transcription by mammalian Mad proteins. *Proceedings of the National Academy of Sciences of the United States of America* 93(23): 12992–12997.

57. Colognato H and Yurchenco PD (2000) Form and function: The laminin family of heterotrimers. *Developmental Dynamics* 218(2): 213–234.

58. Bai KJ, Spicer AP, Mascarenhas MM, et al. (2005) The role of hyaluronan synthase 3 in ventilator-induced lung injury. *American Journal of Respiratory and Critical Care Medicine* 172(1): 92–98.

59. Nagy B Jr, Nagy B, Fila L, et al. (2016) Human epididymis protein 4: A novel serum inflammatory biomarker in cystic fibrosis. *Chest* 150(3): 661–672.

60. Smith P and Heath D (1975) The pathology of the lung in paraquat poisoning. *Journal of Clinical Pathology* 9: 81–93.

61. Vijeyaratnam GS and Corrin B (1971) Experimental paraquat poisoning: A histological and electron-optical study of the changes in the lung. *The Journal of Pathology* 103(2): 123–129.

62. Qi F, Liang ZX, She DY, et al. (2011) A clinical study on the effects and mechanism of Xuebijing injection in severe pneumonia patients. *Journal of Traditional Chinese Medicine* [*Chung I Tsa Chih Ying Wen Pan*] 31(1): 46–49.

63. Gong P, Lu Z, Xing J, et al. (2015) Traditional Chinese medicine Xuebijing treatment is associated with decreased mortality risk of patients with moderate paraquat poisoning. *PLoS ONE* 10(6): e0130508.